Macromolecules

pubs.acs.org/Macromolecules
Article

Flow-Induced Reduction of the Monomeric Friction Coefficient Using a Branched Environment in Linear Isotactic Polypropylene Melt

Jiri Drabek and Martin Zatloukal*

Cite This: Macromolecules 2025, 58, 6041−6051
Read Online

ACCESS | Metrics & More | Article Recommendations | Supporting Information

ABSTRACT: In this work, the effect of the stretch Weissenberg number, Wi_R, on the monomeric friction coefficient is investigated for three entangled linear isotactic polypropylenes (L-PP) and three entangled long-chain branched polypropylene miscible blends (LCB-PP), both groups of polymer melts with a comparable range of the number of Kuhn segments of the whole chain, the number of Kuhn segments between entanglements, the number of entanglements per chain, and the polydispersity index, via free volume measurements using the Williams−Landel−Ferry equation and temperature-dependent high-strain rate rheology (covering the extensional strain rate range of 2×10^4 1/s to 2×10^6 1/s at a Hencky strain of 6.8) via entrance pressure drop measurements in an abrupt contraction flow using the Gibson method. The ratio of the equilibrium monomeric friction coefficient defined by Doi and Edwards, ζ_{eq}, to the monomeric friction coefficient for fully aligned chains due to strong uniaxial extensional flow, $\zeta_{aligned}$, was found to increase in the following order: L-PPs (5.234 ± 0.8489) < 10 wt % LCB-PP blend 64k (6.249 ± 0.3950) < 20 wt % LCB-PP blend 70k (8.061 ± 0.1851) < 30 wt % LCB-PP blend 78k (11.104 ± 0.8995). The presence of a high-molecular-weight branched environment in low-molecular-weight linear PPs caused a more intense decrease in the monomeric friction coefficient (due to the increased free volume indicating a higher coalignment ability of the macromolecules in the LCB-PP blends compared to that of pure linear PP macromolecules), leading to a decrease in the Trouton ratio at Wi_R, in which the polymer chains become fully aligned.

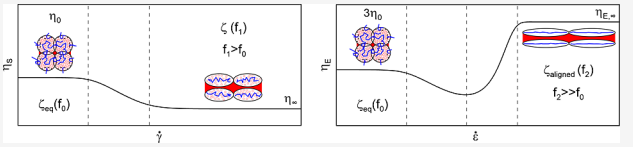

1. INTRODUCTION

The current understanding of polymer melt dynamics in fast flows is mainly based on the concept of a flow-induced reduction of the monomeric friction coefficient, ζ, due to strong orientation and stretching of the polymer chains, in which its value further depends on the chemical structure of the polymer.[1−3] This concept was proposed by Ianniruberto et al.[4,5] and Yaoita et al.[6] In more detail, Ianniruberto and his co-workers considered that the ratio of ζ to its equilibrium value ζ_{eq} is a specific empirical S-shaped function of the Kuhn segment order variable (directly related to stress) with parameters identified using stress-optical data (measured with a modified Meissner-type metal belt rheometer[7]). Yaoita and his colleagues[6] expressed ζ/ζ_{eq} as an implicit function of the stretch/orientation variable (directly related to the subchain stretch ratio and orientational anisotropy of the polymer) and obtained its values using the stress relaxation data obtained after cessation of transient uniaxial extensional flow measured on the Filament Stretching Rheometer (FSR). Following the concept of flow-induced reduction of ζ, Wagner and Narimissa used a generalized tube segment model for entangled chains incorporating the idea of the interchain pressure effect proposed by Marrucci and Ianniruberto[8] to derive a parameter-free expression for ζ/ζ_{eq} that decreases monotonically with chain stretch,[9,10] which was subsequently tested on uniaxial extensional data obtained from FSR measurements.[11] Although their parameter-free friction reduction model was found to behave similarly to the Ianniruberto model,[5] it is unable to describe the ζ/ζ_{eq} saturation at high strain rates. Matsumiya et al.[12] performed a rheo-dielectric test to evaluate the tensor character of ζ (using the Rouse model analysis) from the dielectric loss, viscosity, and first normal stress difference coefficient measured in steady shear flow by using ARES G2 and cone-and-plate geometry. They found that ζ had negligibly small off-diagonal components and ζ was anisotropically reduced at the onset of the shear nonlinearity. In their follow-up study, Matsumiya et al.[13] developed a new theoretical framework for unentangled polymer melts to experimentally asses the ζ in a highly nonlinear shear flow regime via high-shear rheo-dielectric measurements using superimposed oscillatory shear and cone-and-partitioned-plate geometry. A recent theoretical study by Jiang[14] suggested that monomeric coefficients can be related to the projection areas of polymer coils. Assuming that ζ can be viewed as a scalar quantity (i.e., the mean-field frictional coefficient), they related ζ/ζ_{eq} to the basic rheological and structural properties for shear,

Received: March 12, 2025
Revised: April 30, 2025
Accepted: May 23, 2025
Published: June 9, 2025

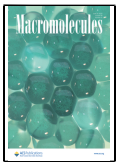

https://doi.org/10.1021/acs.macromol.5c00660
Macromolecules 2025, 58, 6041−6051

Table 1. Basic Molecular Characteristics of Entangled Linear and Branched Polypropylene Melts Taken from refs 46 and 47 Together with Disentangled PP Like Oligomer Called Squalane ($C_{30}H_{62}$; 2,6,10,15,19,23-Hexamethyltetracosane Including Rouse Stretch Time, τ_R, and Equilibrium Monomeric Friction Coefficient, ζ_{eq}, for All Tested PPs at T = 230 °C (N—Number of Kuhn Segments of the Whole Chain; Z—Number of Entanglements per Chain)[c]

sample name	M_n (kg/mol)	$M = M_w$ (kg/mol)	M_z (kg/mol)	M_{z+1} (kg/mol)	M_w/M_n (−)	N^a (−)	Z^b (−)	τ_R (s)	ζ_{eq} (Ns/m)
iPP 56k	14.25	56.25	114.5	187.5	3.947	299.52	8.21	4.296×10^{-6}	7.578×10^{-12}
iPP 64k	14.65	63.75	138.0	235.5	4.352	339.46	9.31	5.074×10^{-6}	6.969×10^{-12}
iPP 76k	17.20	75.85	165.5	278.0	4.410	403.89	11.17	7.746×10^{-6}	7.516×10^{-12}
10 wt % LCB-PP blend 64k	15.20	64.10	139.0	237.0	4.217	341.32	9.36	2.688×10^{-6}	3.651×10^{-12}
20 wt % LCB-PP blend 70k	15.60	69.70	161.5	303.5	4.468	371.14	10.18	3.174×10^{-6}	3.647×10^{-12}
30 wt % LCB-PP blend 78k	17.35	78.15	191.0	373.5	4.504	416.13	11.41	3.787×10^{-6}	3.461×10^{-12}
LCB-PP 247k	36.95	246.50	815.0	1705.0	6.671	1312.57	35.99	3.493×10^{-5}	3.208×10^{-12}
squalane		0.443							

[a]The value is given as M/M_k. [b]The value is given as N/N_e. [c]N_e—number of Kuhn segments between entanglements for all PP samples is the same, given as M_e/M_k = 36.47, where M_e represents the molar mass between entanglements (M_e = 6.850 kg/mol) and M_k is the Kuhn segment molar mass (M_k = 0.1878 kg/mol). M_e and M_k values for iPP were taken from ref 52.

planar extension and uniaxial extension. Despite the simplicity of relationships provided, the experimental identification of the necessary structural data using neutron scattering experiments is a challenging task, as a large facility such as a nuclear reactor serving as a neutron source is required.[12,14]

Although considerable progress has been made in evaluating ζ/ζ_{eq} for polymer melts, the proposed procedures rely on molecular modeling (using a number of assumptions). Also, only nearly monodisperse polymers (such as polystyrenes,[1,2,7,15−26] polyisoprene,[27] poly(*n*-butyl) acrylate,[27] poly(*tert*-butylstyrene),[16,17] poly(propylene carbonate),[10,11,28] poly(*n*-alkyl methacrylate),[16,29,30] poly(2-vinyl naphthalene),[31] poly(4-vinyl biphenyl),[31−33] bottlebrush poly(α-olefins) with side chains ranging from 6 to 16 carbons,[34−36] and linear atactic polypropylene[35,36] melts having high Rouse time, τ_R (typically in order of units to hundreds), are dominantly used to understand the dynamics of polymer melts in very fast extensional flows, since a sufficiently high stretch Weissenberg number ($Wi_R = \dot{\varepsilon}\tau_R \geq 1$) can be easily generated at the low extensional strain rates (typically 0.2−20 1/s at most[15,37]) by the currently used boundary-driven extensional rheometers. However, for polymers with very low τ_R (such as isotactic polypropylene and polyethylenes with τ_R 4 to 6 orders of magnitude lower compared to polystyrenes[38,39]), these rheometers are not applicable due to the limitation of the maximum achievable strain rate. Thus, the current understanding of the dynamics of these polyolefin melts in very fast flows is quite limited due to the absence of relevant experimental data and methodologies to reveal key structure−monomeric friction coefficient−rheology relations. This greatly limits the optimization and development of new polymeric materials used for the production of micro- and nanoproducts through advanced technologies such as meltblown technology, in which extensional strain rates reach 10^6 to 10^7 1/s.[40−42]

To fill this knowledge gap, monomeric friction coefficients for linear isotactic PPs and LCB-PP blends (with a comparable range of the number of Kuhn segments of the whole chain, the number of Kuhn segments between entanglements, the number of entanglements per chain, and the polydispersity index) were determined in this work directly from the free volume measurements using the Williams−Landel−Ferry (WLF) equation and temperature-dependent high-strain rate rheology via flow through an abrupt contraction. The methodology used builds on two previous influential studies by Colby et al.,[43,44] in which monomeric friction coefficients were determined for polymer melts (1,4-polybutadienes, PBDs, having a very wide range of molecular weights)[43] and polymer solutions of various concentrations (high-molecular-weight PBD in phenyloctane)[44] using temperature-dependent zero-shear-rate viscosities and free volumes obtained using the WLF equation. Colby's approach also allows one to understand the viscosity reduction in plasticized polymers through the determination of the free volume and the monomeric friction coefficient, as shown, for example, by Chen et al.,[45] who studied high-molecular-weight polystyrene combined with a small amount of plasticizer (dioctyl phthalate).

The use of WLF and the free volume framework to evaluate monomeric friction coefficients is compatible with the central concept of our understanding of polymer melt dynamics in fast flows, as it characterizes the level of strong orientation and stretching indirectly via the change in free volume, which is a simple scalar variable. Complexity of prior experimental techniques as well as their inapplicability for polymer melts with short Rouse relaxation times (such as iPPs studied in this work) hinders further progress in understanding melt dynamics, which justifies to introduce a new methodology for non-equilibrium conditions based on WLF and free volume framework.

2. EXPERIMENTAL DETAILS

2.1. Materials. Three linear isotactic polypropylenes (PPs [L-PP (76k)—Borflow HL504FB, L-PP (64k)—Borflow HL508FB, and L-PP (56k)—Borflow HL512FB)], high-molecular-weight star-like long chain branched PP [LCB-PP (247k)—Daploy WB180HMS], and three PP miscible blends [containing 10, 20, and 30 wt % of LCB-PP (247k) in low-molecular-weight L-PP (56k)—Borflow HL512FB)], provided by Borealis Polyolefine (Linz, Austria), were used. The basic molecular and rheological characteristics for all tested samples, which were very well characterized in our previous works,[46,47] are summarized in Table 1 and S1 and S2.

Note that the Rouse stretch time, τ_R, and the equilibrium monomeric friction coefficient, ζ_{eq}, for all PPs in Table 1 were determined using Osaki et al.[48] and Doi and Edwards expression,[49−51] respectively, as follows

$$\tau_R = \frac{12M\eta_0}{\pi^2\rho RT}\left(\frac{M_c}{M}\right)^{a-1} \quad (1)$$

$$\zeta_{eq} = \frac{3\pi^2 k_B T}{l^2}\left(\frac{M_k}{M}\right)^2 \tau_R \quad (2)$$

https://doi.org/10.1021/acs.macromol.5c00660
Macromolecules 2025, 58, 6041−6051

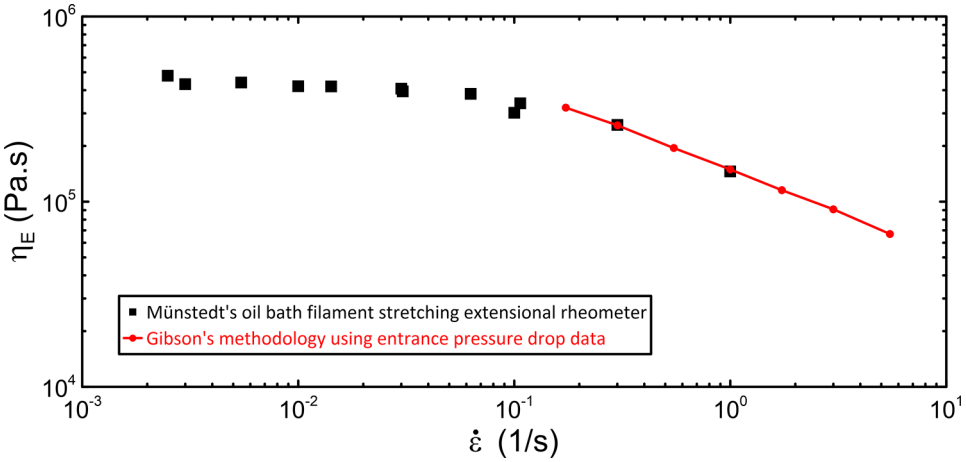

Figure 1. Uniaxial extensional viscosity vs extensional strain rate for linear PP-A measured with Münstedt's oil bath filament stretching rheometer (square symbols—data taken from refs 39, 61−64) compared to η_E obtained from entrance pressure drop data using the Gibson methodology (circle symbols) at T = 180 °C.

where M is the molar mass, M_c is the critical molar mass at which entanglements begins to occur (13.935 kg/mol[38]), η_0 the zero-shear rate viscosity, a represents the slope in the graph of η_0 vs M in the log−log scale where $M > M_c$ (a is 3.620[47] and 4.049[47] for the investigated linear and branched PPs, respectively), ρ the density (766 kg/m^3[52]), R the universal gas constant (8.314 J/K/mol), T the thermodynamic temperature, k_B the Boltzmann constant (1.380649×10^{-23} J/K), l the Kuhn segment length (11.4×10^{-10} m[52]), and M_k the Kuhn segment molar mass (0.1878 kg/mol[52]).

2.2. High Extensional Strain Rate Rheology. The uniaxial extensional viscosity was determined at three different temperatures (190 °C, 210°C, and 230 °C) via entrance pressure drop measurements using a high accuracy Fanuc Roboshot S-2000i electric high-speed injection molding machine equipped with an instrumented rheometric capillary die with an entrance angle $2\alpha = 180° = \pi$ rad[46] and Gibson model.[53−57] Each polymer was injected over a velocity range of 2.6−220 mm/s first through a capillary die of 8 mm length and 0.5 mm diameter, and then the tests were repeated with an orifice die of the same diameter allowing for Bagley and Rabinowitsch corrections. Further details on this instrument and its accuracy are given in ref 58 and the Gibson model used is given as follows

$$\sigma_{xx} = \frac{\overline{P_{Ent}}}{\frac{2}{3k}[1 - (D/D_b)^{3k}] + \frac{\int_0^{\alpha}[1+\cos(\beta)]^{k-1}[\sin(\beta)]^{k+1}\,d\beta}{[\sin(\alpha)(1+\cos(\alpha))]^n}} \quad (3)$$

where σ_{xx} is the uniaxial extensional stress, $\overline{P_{Ent}}$ is the entrance pressure drop without shear contribution defined by eq 4, n is given by eq 5, D is the capillary diameter (0.5 mm), D_b is the barrel diameter (15 mm), α is half the entrance angle ($\pi/2$ rad), and k is given by eq 6.

$$\overline{P_{Ent}} = P_{Ent} - 2\tau_{xy,C}[\sin(\alpha)]^{3n}[1 - (D/D_b)^{3n}][(3n+1)/(4n)]^n /[3n\alpha^{3n+1}] \quad (4)$$

$$n = \frac{d\log(\tau_{xy,C})}{d\log(\dot{\gamma}_A)} \quad (5)$$

$$k = \frac{d\log(\overline{P_{Ent}})}{d\log(\dot{\gamma}_A)} \quad (6)$$

where P_{Ent} is the measured entrance pressure drop, $\tau_{xy,C}$ is the Bagley-corrected wall shear stress, and $\dot{\gamma}_A$ is the apparent shear rate. The uniaxial extensional viscosity is defined as

$$\eta_E = \frac{\sigma_{xx}}{\dot{\varepsilon}} \quad (7)$$

where the $\dot{\varepsilon}$ is the extensional strain rate given by eq 8.

$$\dot{\varepsilon} = \frac{1}{4}\dot{\gamma}_A \sin(\alpha)[1 + \cos(\alpha)] \quad (8)$$

The maximum attainable Hencky strain for the used abrupt contraction flow geometry is given by refs 59 and 60 as follows

$$\varepsilon_{max} = 2\ln\left(\frac{D_b}{D}\right) \quad (9)$$

where D_b (= 15 mm) is the barrel diameter and D (= 0.5 mm) is the orifice die diameter. According to eq 9, ε_{max} is 6.8 in this case.

To confirm the accuracy of the chosen Gibson methodology for measuring the uniaxial extensional viscosity, we performed measurements at low extensional strain rates on a Rosand RH10 high pressure capillary rheometer with D_b = 15 mm (using capillary die 32 mm long and 2 mm in diameter, FreeFlow orifice die[55] of the same diameter, and 1500PSI and 250PSI pressure transducers calibrated to their resolution limit) for a very well-characterized linear PP-A melt (M_n = 159 kg/mol, M_w = 669 kg/mol, M_z = 1654 kg/mol, PDI = 4.20[61−64]), and the obtained results were compared with the corresponding uniaxial extensional viscosity data for the same PP-A melt measured on the Münstedt's oil bath Filament Stretching Rheometer (FSR), which are available in the open literature[39,61−64] (see Figure 1).

As can be seen, the chosen Gibson methodology agrees well with Münstedt's oil bath FSR uniaxial extensional viscosity data for linear PP melt, justifying its use for high extensional strain rate rheology for PP samples considered in this work.

2.3. Monomeric Friction Coefficient from Flow-Induced Change in Free Volume. Doolittle[65−68] showed that the free volume as the only parameter in determining the molecular mobility governs the viscosity of liquids using the following equation

$$\eta = A\exp\left(\frac{B}{\Phi}\right) \quad (10)$$

where A and B are empirical constants (B around unity) and Φ is the "relative free volume" defined as

$$\Phi = \frac{v_f}{v_0} \quad (11)$$

Here, the free volume, $v_f = v - v_0$, is given by the measured volume v and inaccessible volume v_0. The physical meaning of eq 10 can be understood through the molecular transport theory of liquids proposed by Cohen and Turnbull,[68,69] in which the self-diffusion of a spherical molecule, which is directly proportional to the fluidity ϕ (defined as $1/\eta$), occurs only when the void size reaches a critical size to which the molecule can move. This critical void size is close to the occupied volume per molecule or the volume per some kind of segmental unit when considering a polymer chain instead of a single spherical

https://doi.org/10.1021/acs.macromol.5c00660
Macromolecules 2025, 58, 6041−6051

molecule[67]). When Williams, Landel, and Ferry rationalized their WLF equation for the temperature shift factor a_T to Doolittle's free volume theory, they chose to use the "fractional free volume" $f = v_f/v$ in place of Φ considering v_0 as a sum of macromolecules volume (determined by their van der Waals radii and thermal vibrational motions) and v_f as the excess free volume, which can be represented as holes of molecular (monomeric) dimensions.[67,70] Assuming that the slow temperature variation of the temperature-density product, $T\rho$, can be neglected (i.e., that modulus scale shift factor ≈1), they obtained the following formula for a_T

$$a_T = \frac{\eta(f)}{\eta(f_0)} = \exp\left[B\left(\frac{1}{f} - \frac{1}{f_0}\right)\right] \tag{12}$$

where $\eta(f)$ and $\eta(f_0)$ represent viscosities obtained at a given and a reference fractional free volume, respectively.[67] Note that using f instead of Φ made no difference in their derivation, because $(1/f - 1/f_0) = (1/\Phi - 1/\Phi_0)$.[71] Ferry[67] also showed that the expression for the same a_T also applies to the monomeric friction coefficient ratio

$$a_T = \frac{\zeta(f)}{\zeta(f_0)} \tag{13}$$

Since the free volume f increases due to flow-induced coalescence of shaped free volume cavities[47,72] and also linearly with temperature,[67] f can be expressed as

$$f = f_0 + \alpha_f(T - T_0) \tag{14}$$

where f_0 represents the free volume at a reference strain rate (which may or may not cause the chain stretch) and at a reference temperature T_0 and α_f is the thermal expansion coefficient of the free volume. There may be various mathematical expressions for f_0 that would express the functional dependence on temperature and strain rate (or Weissenberg number), but their derivation and testing are beyond the scope of this experimental work. The combination of eqs 12 and 14 leads to the following expression for the shift factor a_T

$$a_T = 10^{-\frac{d_1(T-T_0)}{d_2+(T-T_0)}} \tag{15}$$

where d_1 and d_2 are related to f_0, α_f, and B as follows

$$\frac{f_0}{B} = \frac{\log e}{d_1} = \frac{1}{2.303 d_1} \tag{16}$$

$$\frac{\alpha_f}{B} = \frac{\log e}{d_1 d_2} = \frac{1}{2.303 d_1 d_2} \tag{17}$$

Equation 15 is the well-known WLF equation.[67] The shift factor a_T was expressed using a base of 10 rather than a base of e (Euler's number) because the decimal rather than the natural logarithm is commonly used to quantify the strain rate dependence of viscosity. Since f_0 is assumed to be associated with some strain rate reference value, we use the notation $f_0(\dot{\gamma})$ and $f_0(\dot{\varepsilon})$ when considering shear and extensional flow, respectively. In this work, we used the WLF equation for low strain rate viscosity data (where chain stretch does not occur) and also for high strain rate viscosity data (where chain stretching is present) to determine the free volume-dependent friction coefficient using $\alpha_f f_0(\dot{\gamma})$ and $f_0(\dot{\varepsilon})$ in the following way.

2.3.1. Determination of Free Volume Parameters from Shear Flow. The reference amount of fractional free volume $f_0(\dot{\gamma} \to 0)/B$ was determined under equilibrium flow conditions without chain stretch (i.e., at the zero-shear rate) using a shift factor $a_{T,0}$ given as

$$a_{T,0} = \frac{\eta_0(T)}{\eta_0(T_0)} \tag{18}$$

where $\eta_0(T)$ and $\eta_0(T_0)$ are the zero-shear viscosity at the actual and reference temperature, respectively. In this case, the experimentally determined $a_{T,0}$ can be described by the WLF equation, where $f_0 = f_0(\dot{\gamma} \to 0)$. The free volume parameter induced by chain stretching due to shear, $f_0(\dot{\gamma} \to \infty)/B$, was determined from the measured limiting high shear rate viscosity, η_∞, obtained at shear rates between 2×10^6 and 7×10^6 1/s [see Figure 5 in ref 46—i.e., in the range of the stretch Weissenberg numbers Wi_R ($= \tau_R\dot{\gamma}$) between approximately 10 and 50] using the following shift factor $a_{T\infty}$

$$a_{T,\infty} = \frac{\eta_\infty(T)}{\eta_\infty(T_0)} \tag{19}$$

In this case, $a_{T,\infty}$ can be described by the WLF equation where $f_0 = f_0(\dot{\gamma} \to \infty)$. Temperature-dependent η_0 and η_∞ experimental data for all tested samples are summarized along with $a_{T,0}$ and $a_{T,\infty}$ values in Tables S1 and S2. It should be mentioned that the use of eq 19 is justified because η_∞ values were determined for all samples from the measured high shear rate plateau regions in the shear viscosity vs shear rate plots, i.e., where the shear viscosity does not change with shear rate (for further details, see our previous works[46,47]). The WLF equation was used to simultaneously fit both shift factors to obtain $\alpha_f/B, f_0(\dot{\gamma} \to 0)/B$, and $f_0(\dot{\gamma} \to \infty)/B$ using $T_0 = 230$ °C and assuming that α_f/B is the same for all tested samples. Comparison between the generalized WLF equation fits and the corresponding shift factors for all tested samples is shown in Figures S1−S3, and the obtained parameters are summarized in Table 2.

Table 2. Thermal Expansion Coefficient of the Free Volume α_f/B, Equilibrium Fractional Free Volume $f_0(\dot{\gamma} \to 0)/B$ Determined from η_0, and Maximum Achievable Fractional Free Volume $f_0(\dot{\gamma} \to \infty)/B$ due to Chain Stretching Induced by Shear Flow Determined From η_∞ at Reference Temperature T_0 = 230 °C

material	α_f/B (1/K)	$f_0(\dot{\gamma} \to 0)/B$ (−)	$f_0(\dot{\gamma} \to \infty)/B$ (−)
iPP 56k[b]	1.470×10^{-3}[c]	0.260 ± 0.0031	0.381 ± 0.0009
iPP 64k[b]		0.256 ± 0.0048	0.372 ± 0.0045
iPP 76k[b]		0.261 ± 0.0046	0.395 ± 0.0042
10 wt % LCB-PP blend 64k		0.258 ± 0.0003	0.383 ± 0.0029
20 wt % LCB-PP blend 70k		0.257 ± 0.0014	0.387 ± 0.0048
30 wt % LCB-PP blend 78k		0.254 ± 0.0002	0.387 ± 0.0211
squalane		0.403 ± 0.0138[a]	

[a]The mean and standard deviation for squalane were determined from zero-shear rate viscosity measurements at 1, 20, 40, 60, 80, 100, 120, 140, and 160 MPa taken from ref 73 using a reference temperature of 200 °C (for more details, see Figure S2 and Tables S3a,b). [b]$f_0(\dot{\gamma} \to 0)/B = 0.258 \pm 0.0043$ and $f_0(\dot{\gamma} \to \infty)/B = 0.383 \pm 0.0102$ represent average values from all three iPPs. [c]The value is the same for all samples.

2.3.2. Determination of the Free Volume Parameter from Uniaxial Extensional Flow. The free volume parameter induced by chain stretching due to uniaxial extensional flow, $f_0(\dot{\varepsilon})/B$, was determined from uniaxial extensional viscosities measured at extensional strain rates in the range of 2×10^4 1/s to 2×10^6 1/s [i.e., in the range of the stretch Weissenberg numbers Wi_R ($= \tau_R\dot{\varepsilon}$) between about 10^{-1} and 10] using a shift factor

$$a_{T,E} = \frac{\eta_E(T, \dot{\varepsilon})}{\eta_E(T_0, \dot{\varepsilon}_0)} = \frac{\dot{\varepsilon}_0(T_0)}{\dot{\varepsilon}(T)} \tag{20}$$

where $\eta_E(T, \dot{\varepsilon})$ and $\eta_E(T_0, \dot{\varepsilon}_0)$ are the uniaxial extensional viscosity at the actual and reference temperature and extensional strain rate, respectively. In this case, $a_{T,E}$ can be described by the WLF equation, where $f_0 = f_0(\dot{\varepsilon})$, i.e., the shift factor can vary with the extensional strain rate, $\dot{\varepsilon}$, satisfying eq 20.[67] The measured uniaxial extensional viscosity data as a function of strain rate and temperature for all tested samples are visualized in Figure 2 and summarized along with the corresponding $a_{T,E}$ values in Tables S4−S9.

https://doi.org/10.1021/acs.macromol.5c00660
Macromolecules 2025, 58, 6041−6051

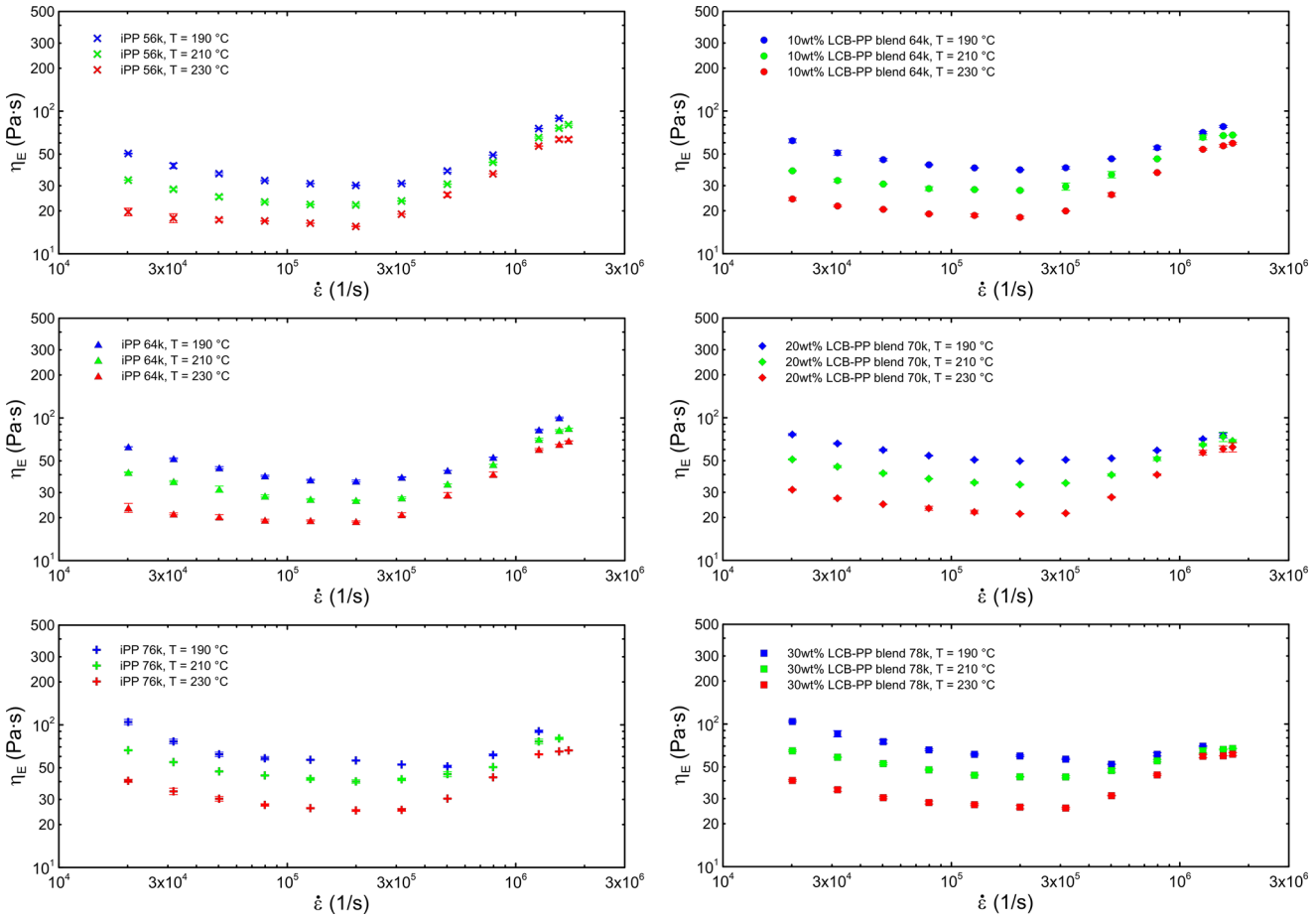

Figure 2. Uniaxial extensional viscosity plotted as a function of extensional strain rate for three linear iPPs (PP 56k—top left, PP 64k—middle left, PP 76k—bottom left) and three branched PPs (10 wt % LCB-PP blend 64k—top right, 20 wt % LCB-PP blend 70k—middle right, 30 wt % LCB-PP blend 78k—bottom right) at three different temperatures. All data are provided in Tables S4–S9.

The WLF equation was used to simultaneously fit the temperature and extensional strain rate-dependent $a_{T,E}$ to obtain $f_0(\dot{\varepsilon})/B$ for each strain rate using T_0 = 230 °C and $\alpha_f/B = 1.470 \times 10^{-3}$ 1/K. Note that Gibson's methodology provides a temperature-independent $\dot{\varepsilon}$ (see eq 8), which allows $f_0(\dot{\varepsilon})/B$ to be determined directly (i.e., without the need to interpolate values of extensional viscosity measured at different temperatures to a given fixed value of $\dot{\varepsilon}$). Comparison between the WLF equation fits and the corresponding $a_{T,E}$ values for all tested samples and strain rates are shown in Figures S4 and S5; the resulting mastercurves ($\eta_E/a_{T,E}$ vs $\dot{\varepsilon}\ a_{T,E}$) are provided in Figure 3 and the $f_0(\dot{\varepsilon})/B$ values obtained are summarized in Tables S10 and S11.

In order to express the free volume change induced by uniaxial extensional flow, $\Delta f_0(\dot{\varepsilon})/B$ was calculated as the difference between $f_0(\dot{\varepsilon})/B$ and the equilibrium fractional free volume $f_0(\dot{\gamma} \to 0)/B$ (see Table 2) and plotted in Figure 4 as a function of the extensional strain rate at reference temperature T_0 = 230 °C for all tested samples.

The same dependence for $f_0(\dot{\varepsilon})/B$ is also shown in Figure S6. As can be seen, the maximum achievable fractional free volume $f_0(\dot{\varepsilon} \to \infty)/B$ can be obtained at $\dot{\varepsilon} \sim 10^6$ 1/s, where $f_0(\dot{\varepsilon})/B$ becomes independent of the strain rate. These values are summarized in Table 3.

2.3.3. Determination of the Monomeric Friction Coefficient. The equation for the free volume-dependent monomeric friction coefficient, $\zeta(f)$, at a given temperature can be obtained by combining eqs 12 and 13, which gives

$$\zeta(f) = \zeta(f_0)\exp\left[B\left(\frac{1}{f} - \frac{1}{f_0}\right)\right] \tag{21}$$

where f_0 represents the reference value of the fractional free volume at the equilibrium flow conditions [$f_0 = f_0(\dot{\gamma} \to 0)$] and f represents the increased fractional free volume due to flow-induced chain stretch and subsequent coalescence of shaped free volume cavities [where $f = f_0(\dot{\gamma} \to \infty)$ or $f_0(\dot{\varepsilon})$ depending on whether chain stretching causes shear or extensional flow].

The values summarized in Table 2 for $f_0(\dot{\gamma} \to 0)/B$ and $f_0(\dot{\gamma} \to \infty)/B$ in eq 21 make it possible to directly calculate the maximum achievable $(\zeta_{eq}/\zeta_{aligned})_{Shear} = \zeta[f_0(\dot{\gamma} \to 0)]/\zeta[f_0(\dot{\gamma} \to \infty)]$ ratio in the shear flow at the reference temperature T_0 = 230 °C. For linear PPs, the following average values were used for the given calculation: $f_0(\dot{\gamma} \to 0)/B = 0.258 \pm 0.0043$ and $f_0(\dot{\gamma} \to \infty)/B = 0.383 \pm 0.0102$.

The extensional strain rate-dependent $\zeta[f_0(\dot{\varepsilon} \to 0)]/\zeta[f_0(\dot{\varepsilon})]$ ratio for uniaxial extensional flow was determined using $f_0(\dot{\varepsilon})/B$ values given in Tables S10 and S11 for the given extensional strain rates, polymer samples, and reference temperature T_0 = 230 °C and are summarized in Tables S14 and S15. Here, $f_0(\dot{\varepsilon} \to 0)/B$ is equal to $f_0(\dot{\gamma} \to 0)/B$ considering the validity of Trouton's relation. The maximum achievable $(\zeta_{eq}/\zeta_{aligned})_{Elongation} = \zeta[f_0(\dot{\varepsilon} \to 0)]/\zeta[f_0(\dot{\varepsilon} \to \infty)]$ ratio in uniaxial extensional flow was determined using the $f_0(\dot{\varepsilon} \to \infty)/B$ values summarized in Table 3, which were obtained from the highest extensional strain rates at which the chain stretch-induced free volume parameter becomes constant (see dashed lines in Figure 4). For linear PPs, the following average values were used for the calculation: $f_0(\dot{\varepsilon} \to 0)/B = 0.258 \pm 0.0043$ and $f_0(\dot{\varepsilon} \to \infty)/B = 0.455 \pm 0.0336$. The obtained $(\zeta_{eq}/\zeta_{aligned})_{Shear}$ and $(\zeta_{eq}/\zeta_{aligned})_{Elongation}$ values are summarized in Table 4, which represents the main result of this work.

https://doi.org/10.1021/acs.macromol.5c00660
Macromolecules 2025, 58, 6041−6051

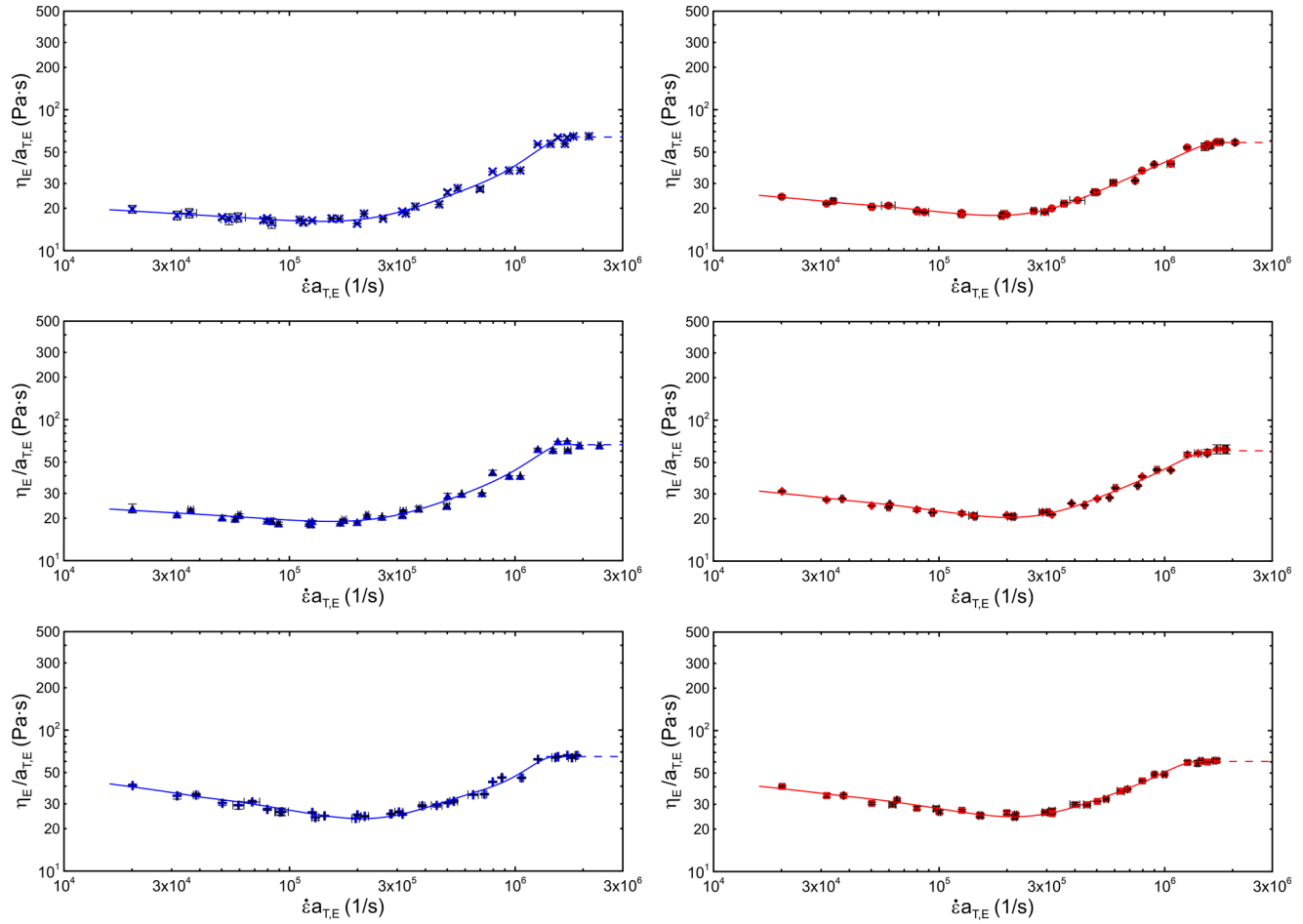

Figure 3. Master curve for uniaxial extensional viscosity plotted as a function of the extensional strain rate for three linear iPPs (PP 56k—top left, PP 64k—middle left, PP 76k—bottom left) and three branched PPs (10 wt % LCB-PP blend 64k—top right, 20 wt % LCB-PP blend 70k—middle right, 30 wt % LCB-PP blend 78k—bottom right).

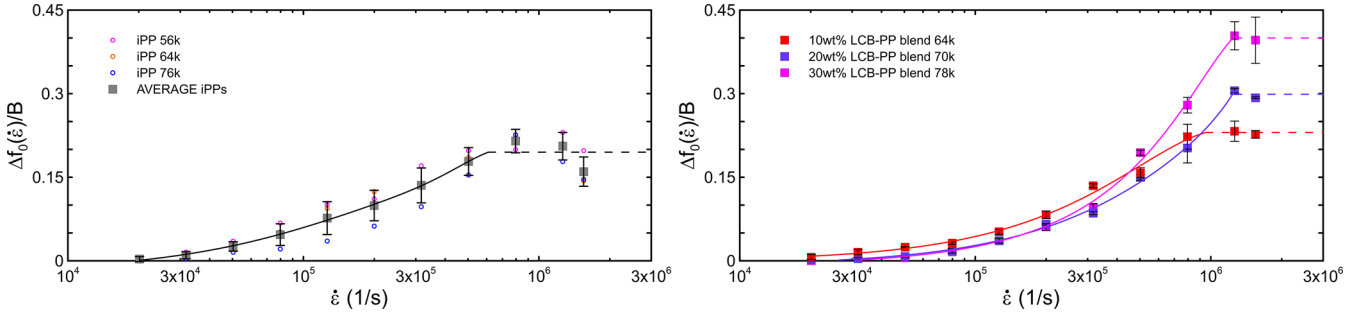

Figure 4. Chain stretch-induced free volume plotted as a function of extensional strain rate for linear left) and branched PPs (right) at a reference temperature 230 °C. All data are provided in Tables S12 and S13.

3. RESULTS AND DISCUSSION

Based on the results summarized in Table 2, it can be seen that first, the maximum achievable chain stretching due to shear (i.e., when $\dot{\gamma} \rightarrow \infty$) causes an increase in the fractional free volume of tested samples between 45 and 52% compared to equilibrium conditions without the chain stretching (that is, when $\dot{\gamma} \rightarrow 0$). This can be attributed to the coalescence of the free volume cavities due to the shear-induced chain stretching.

Second, the equilibrium fractional free volume parameter $f_0(\dot{\gamma} \rightarrow 0)/B$ for linear PPs appears to be slightly higher (mean 0.259) than that for LCB-PP blends (mean 0.256), which can be attributed to the easier coalescence of free volume cavities due to the lower level of entanglements in linear PPs compared to that in LCB-PP blends. On the other hand, the chain stretch-induced free volume parameter due to strong shear (causing entanglements to disappear) $f_0(\dot{\gamma} \rightarrow \infty)/B$ for LCB-PP blends (mean 0.386) appears to be slightly higher than that of linear PPs (mean 0.383), indicating a more dominant coalescence of free volume cavities compared to linear PPs (probably due to the smaller radius of gyration of LCB-PPs compared to that of their linear counterparts[47]).

Third, a polypropylene-like oligomer without chain entanglements (squalane, $C_{30}H_{62}$; 2,6,10,15,19,23-hexamethyltetracosane) has $f_0(\dot{\gamma} \rightarrow 0)/B$ (mean 0.403) much higher (about 55%)

https://doi.org/10.1021/acs.macromol.5c00660
Macromolecules 2025, 58, 6041−6051

Table 3. Maximum Achievable Fractional Free Volume $f_0(\dot{\varepsilon} \rightarrow \infty)/B$ Due to Uniaxial Extensional Flow Induced Chain Stretch at Reference Temperature T_0 = 230 °C Using α_f/B = 1.470 × 10^{-3} 1/K

material	$f_0(\dot{\varepsilon} \rightarrow \infty)/B$ (−)
iPP 56k[a]	0.477 ± 0.0162
iPP 64k[a]	0.433 ± 0.0352
iPP 76k[a]	0.423 ± 0.0212
10 wt % LCB-PP blend 64k	0.488 ± 0.0151
20 wt % LCB-PP blend 70k	0.556 ± 0.0071
30 wt % LCB-PP blend 78k	0.654 ± 0.0346

[a] $f_0(\dot{\varepsilon} \rightarrow \infty)/B$ = 0.455 ± 0.0336 represents the average values from all three iPPs.

Table 4. Maximum Achievable $\zeta_{eq}/\zeta_{aligned}$ Ratio in Shear and Uniaxial Extensional Flow for the Tested PPs at T = 230 °C

material	$(\zeta_{eq}/\zeta_{aligned})_{Shear}$ (−)	$(\zeta_{eq}/\zeta_{aligned})_{Elo}$ (−)
iPP 56k	3.483 ± 0.1608[a]	5.234 ± 0.8489[a]
iPP 64k		
iPP 76k		
10 wt % LCB-PP blend 64k	3.571 ± 0.0587	6.249 ± 0.3950
20 wt % LCB-PP blend 70k	3.684 ± 0.1179	8.061 ± 0.1851
30 wt % LCB-PP blend 78k	3.964 ± 0.5488	11.104 ± 0.8995

[a] The value is the same for all three iPP samples.

compared to $f_0(\dot{\gamma} \rightarrow 0)/B$ of entangled linear PPs and LCB-PP blends, as expected. However, $f_0(\dot{\gamma} \rightarrow 0)/B$ of squalane is comparable to $f_0(\dot{\gamma} \rightarrow \infty)/B$, confirming that the linear PPs and LCB-PP blends are completely disentangled when the shear stretch Weissenberg number Wi_R (= $\tau_R\dot{\gamma}$) is higher than 10. These conclusions are consistent with our previous work based on the analysis of flow activation energies using the Arrhenius equation.[46,47] It is important to mention that the chain scission may occur during the fast flows of PP melts as shown in our previous works.[46,47] Therefore, to maintain a clear relationship between the molecular structure and measured rheological data for all tested PPs, molecular weight distribution and average molecular weights M_n, M_w, M_z, and M_{z+1} provided in Table 1 were measured using high-temperature gel permeation chromatography on PP samples rheologically evaluated at high strain rates, which were then used for low strain rate measurements on a rotational rheometer to determine zero-shear rate viscosity.[46,47] The fact that infinite shear viscosities scale linearly with the weight average molecular weight, M_w, for all tested iPP samples, while zero-shear viscosities scale with M_w^a (where a = 3.620 for linear PPs a = 4.049 for LCB-PP blends)—see Figure 4 in ref 47, further supports the statement that "the linear PPs and LCB-PP blends are completely disentangled" in very fast flows but become fully entangled at weak flows.

In uniaxial extensional flow, there is practically no change in the free volume and monomeric friction coefficients up to the end of the extensional thinning region, i.e., to $\dot{\varepsilon}$ = 5 × 10^4 s^{-1}, which corresponds to stretch Weissenberg numbers Wi_R (= $\tau_R\dot{\varepsilon}$) equal to about 0.3, as seen in Figures 4 and 5 and S6. This indicates that flow-induced chain disentanglements, which cause extensional thinning, have virtually no effect on the free volume and monomer friction coefficients. The $f_0(\dot{\varepsilon})/B$, $\Delta f_0(\dot{\varepsilon})/B$, and $\zeta[f_0(\dot{\varepsilon} \rightarrow 0)]/\zeta[f_0(\dot{\varepsilon})]$ start to increase considerably at the stretch Weissenberg numbers Wi_R (= $\tau_R\dot{\varepsilon}$) equal to 1 (i.e., about $\dot{\varepsilon}$ = 3 × 10^5 s^{-1}) and become constant between 5 and 10 (i.e., above about $\dot{\varepsilon}$ = 10^6 s^{-1}), as shown in Figures 4, 5, and S6. This suggests that chain stretch is a key factor controlling the change in free volume and the monomer friction coefficient.

It was found that the maximum achievable fractional free volume $f_0(\dot{\varepsilon} \rightarrow \infty)/B$ parameters, which are summarized in Table 3 for all tested samples, increase in the following order: Linear PPs (0.455 ± 0.0336) < 10 wt % LCB-PP blend 64k (0.488 ± 0.0151) < 20 wt % LCB-PP blend 70k (0.556 ± 0.0071) < 30 wt % LCB-PP blend 78k (0.654 ± 0.0346), i.e., the flow-induced free volume is higher for LCB-PP blends compared to their linear counterparts. However, there are differences when compared with $f_0(\dot{\gamma} \rightarrow \infty)/B$. First, $f_0(\dot{\varepsilon} \rightarrow \infty)/B > f_0(\dot{\gamma} \rightarrow \infty)/B$, and second, $f_0(\dot{\varepsilon} \rightarrow \infty)/B$ increases with the weight percent of the branched component in LCB-PP blends, while $f_0(\dot{\gamma} \rightarrow \infty)/B$ does not, i.e., only $f_0(\dot{\varepsilon} \rightarrow \infty)/B$ can differentiate between the tested samples. Both observations can be understood through the increased coalescence of free volume cavities in the uniaxial extensional flow, which allows a significantly larger extension of polymer chains to be achieved than that in shear flow. The observed increase in the free volume parameter $f_0(\dot{\varepsilon} \rightarrow \infty)/B$ due to increased wt % of the branched high-molecular-weight component in LCB-PP blends could be understood via the significant alignment of the chain branches along the backbone as well as the backbone itself (i.e., which can be considered as an environment for linear PP chains) promoting the coalescence of free volume cavities.

As can be seen from Table 4, $(\zeta_{eq}/\zeta_{aligned})_{Elongation} > (\zeta_{eq}/\zeta_{aligned})_{Shear}$, their difference is higher for LCB-PP blends compared to that for linear PPs, and finally, the increase in the wt % content of the branched component in LCB-PP blends causes an increase in $(\zeta_{eq}/\zeta_{aligned})_{Elongation}$, which also seems to be valid

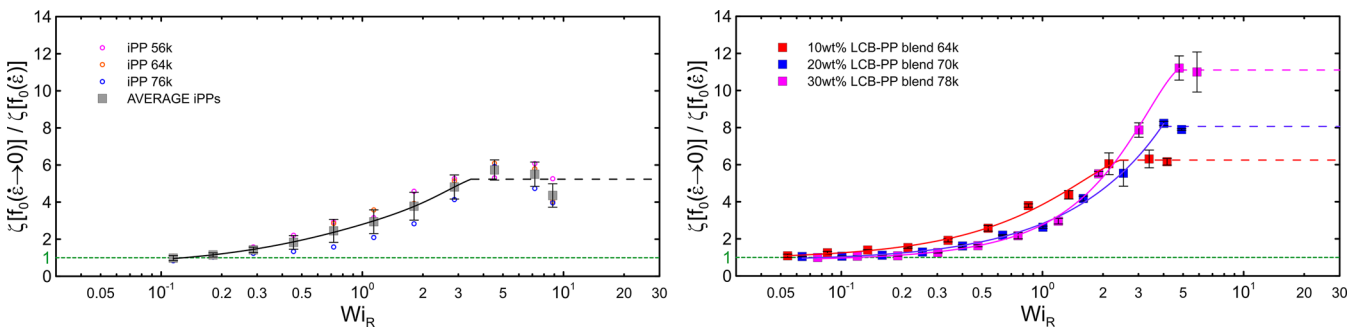

Figure 5. Ratio of equilibrium friction coefficient to uniaxial extensional flow reduced friction coefficient plotted as a function of the stretch Weissenberg number Wi_R (= $\tau_R\dot{\gamma}$) for linear (left) and branched PPs (right) at a reference temperature of 230 °C. All data are provided in Tables S14 and S15.

https://doi.org/10.1021/acs.macromol.5c00660
Macromolecules 2025, 58, 6041−6051

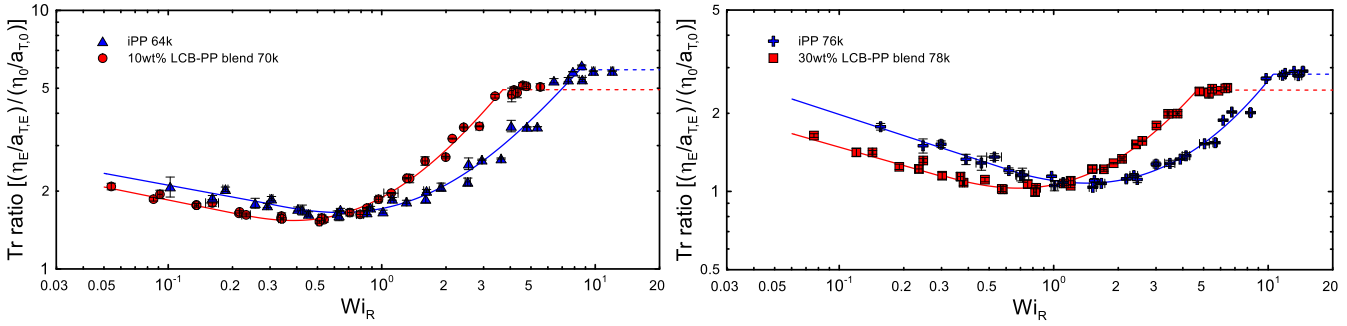

Figure 6. Master curve for the Trouton ratio plotted as a function of the stretch Weissenberg number Wi_R ($= \tau_R a_{T,E} \dot{\epsilon}$) at a reference temperature of 230 °C for pairs of linear and branched PPs with a comparable range of the number of Kuhn segments of the whole chain, the number of Kuhn segments between entanglements, the number of entanglements per chain, and the polydispersity index [left—iPP 64k (N = 339.46, N_e = 36.47, Z = 9.31) and 10 wt % LCB-PP blend 64k (N = 341.32, N_e = 36.47, Z = 9.36); right—iPP 76k (N = 403.89, N_e = 36.47, Z = 11.07) and 30 wt % LCB-PP blend 78k (N = 416.13, N_e = 36.47, Z = 11.41)]. All data are provided in Tables S16 and S17.

for $(\zeta_{eq}/\zeta_{aligned})_{Shear}$. Interestingly, the average $(\zeta_{eq}/\zeta_{aligned})_{Elongation}$ value obtained for linear PPs in this work (i.e., 5.234 ± 0.8489) is close to the values obtained in our previous work (2.9−5 considering that $M = M_w$[38]) for the same PPs using an expression relating a high-strain-rate limiting value of uniaxial extensional viscosity with $\zeta_{aligned}$ derived in ref 1 for a fully stretched Fraenkel chain. The effect of branched components on linear PP chains in LCB-PP blends leading to an increase in $(\zeta_{eq}/\zeta_{aligned})_{Elongation}$ can be understood by nematic (orientational) interactions, which were found to cause a decrease in the monomeric friction coefficient of polystyrene molecules in an oligomeric styrene solvent with increased size of used oligomers.[20,74] In more detail, the presence of a high-molecular-weight branched environment in low-molecular-weight linear PPs appears to cause a high coalignment of macromolecules in LCB-PP blends, leading to more intense coalescence of free volume cavities compared to pure linear PP melts. This hypothesis can be supported, first, by the fact, that the maximum achievable $(\zeta_{eq}/\zeta_{aligned})_{Elongation}$ for LCB-PP blends is reached at smaller stretch Weissenberg numbers (critical Wi_R is about 5) compared to that for linear PPs (critical Wi_R is about 10) (see Figure 5). The same trend can also be observed for the Trouton ratio plotted in Figure 6 as a function of Wi_R at the reference temperature T_0 = 230 °C for two pairs of samples that have a comparable range of the number of Kuhn segments of the whole chain, the number of Kuhn segments between entanglements, the number of entanglements per chain, and the polydispersity index [first—iPP 64k (N = 339.46, N_e = 36.47, Z = 9.31) and 10 wt % LCB-PP blend 64k (N = 341.32, N_e = 36.47, Z = 9.36); second—iPP 76k (N = 403.89, N_e = 36.47, Z = 11.07) and 30 wt % LCB-PP blend 78k (N = 416.13, N_e = 36.47, Z = 11.41)].

It can also be seen that the increase in $(\zeta_{eq}/\zeta_{aligned})_{Elongation}$ due to the addition of the branched component to the linear PP melt decreases the Trouton ratio similar to the addition of a high-molecular-weight oligomeric solvent to a polystyrene solution, where the reduction in friction was attributed to flow-induced nematic interactions between the polymer and the chemical structure and size of the molecules forming their environment.[20,73]

It is interesting to note that although the strain rates in this work are very high, the corresponding Wi_R numbers are not very large (up to 10). For other samples such as polystyrene (PS), poly(methyl methacrylate) (PMMA), and poly(tert-butylstyrene) (PtBS) melts, at Wi_R = 10, the extensional viscosity has no sign to turn to a constant regime (see Figure 8b in ref 16). An interesting question might be why PP melt chains reach a fully aligned state so easily. It seems that the fully aligned state achieved at the very high strain rates used in this work is directly related to the complete disentanglement of polymeric chains, suggesting that both high strain rates for complete disentanglement of polymer chains and sufficiently high Wi_R numbers are required to achieve a fully aligned state. The observation that other samples, such as PS, PMMA, and PtBS melts do not exhibit a constant regime when the Wi_R number is high can therefore be attributed to the low extensional strain rates used (0.01−0.6 1/s[16]), which are not high enough to reach a complete disentanglement state.

4. CONCLUDING REMARKS

In this work, the effect of the Wi_R (varying from 10^{-1} to 10) on the monomeric friction coefficient for linear PPs and LCB-PP blends (with a comparable range of the number of Kuhn segments of the whole chain, the number of Kuhn segments between entanglements, the number of entanglements per chain, and the polydispersity index) was investigated by measuring the free volume using the WLF equation and temperature-dependent high-strain rate rheology. The flow through an abrupt contraction and the Gibson method were used to measure uniaxial extensional viscosities. It was found that the maximum achievable $\zeta_{eq}/\zeta_{aligned}$ ratio, achieved at Wi_R between 5 and 10 for all tested samples, increased in the following order: Linear PPs (5.234 ± 0.8489) < 10 wt % LCB-PP blend 64k (6.249 ± 0.3950) < 20 wt % LCB-PP blend 70k (8.061 ± 0.1851) < 30 wt % LCB-PP blend 78k (11.104 ± 0.8995). It was revealed that the presence of a high-molecular-weight branched environment in low-molecular-weight linear PPs causes, first, a more intense increase in free volume (probably due to chain-stretch induced coalescence of free volume cavities and a higher coalignment ability of macromolecules in LCB-PP blends) compared to pure linear PP macromolecules and, second, a reduction of the Trouton ratio at Wi_R, at which the polymer chains become fully aligned.

■ ASSOCIATED CONTENT

Supporting Information

The Supporting Information is available free of charge at https://pubs.acs.org/doi/10.1021/acs.macromol.5c00660.

https://doi.org/10.1021/acs.macromol.5c00660
Macromolecules 2025, 58, 6041−6051

Temperature-dependent zero-shear rate viscosities, η_0, infinite shear viscosities, η_∞, WLF model fits and corresponding shift factors $a_{T,0}$ and $a_{T,\infty}$, experimental data for strain-rate-and temperature-dependent uniaxial extensional viscosities, shift factors, $a_{T,E}$, and corresponding generalized WLF model fits, fractional free volumes, $f_0(\dot{\varepsilon})/B$, chain stretch-induced free volumes, $\Delta f_0(\dot{\varepsilon})/B$, ratios of equilibrium friction coefficient to uniaxial extensional flow reduced friction coefficient $\zeta[f_0(\dot{\varepsilon} \to 0)]/\zeta[f_0(\dot{\varepsilon})]$, and Weissenberg number-dependent Trouton ratios (PDF)

AUTHOR INFORMATION

Corresponding Author

Martin Zatloukal − *Department of Polymer Engineering, Faculty of Technology, Tomas Bata University in Zlin, 760 01 Zlin, Czech Republic;* orcid.org/0000-0003-1894-2103; Email: mzatloukal@utb.cz

Author

Jiri Drabek − *Department of Polymer Engineering, Faculty of Technology, Tomas Bata University in Zlin, 760 01 Zlin, Czech Republic*

Complete contact information is available at: https://pubs.acs.org/10.1021/acs.macromol.5c00660

Notes

The authors declare no competing financial interest.

ACKNOWLEDGMENTS

The authors wish to acknowledge Grant Agency of the Czech Republic (Grant registration No. 24-11442S) for financial support. The authors also wish to acknowledge Helmut Münstedt and Joachim Kaschta from Friedrich-Alexander-University Erlangen-Nürnberg (Erlangen, Germany) for the donation of the PP-A sample, Jiří Juračka for his help during rheological evaluation of the PP-A sample, and Levente Szántó from Netzsch Gerätebau (Selb, Germany) for his support.

REFERENCES

(1) Ianniruberto, G.; Marrucci, G.; Masubuchi, Y. Melts of linear polymers in fast flows. *Macromolecules* **2020**, *53* (13), 5023−5033.

(2) Matsumiya, Y.; Watanabe, H. Non-universal features in uniaxially extensional rheology of linear polymer melts and concentrated solutions: A review. *Prog. Polym. Sci.* **2021**, *112*, 101325.

(3) Huang, Q. When polymer chains are highly aligned: A perspective on extensional rheology. *Macromolecules* **2022**, *55* (3), 715−727.

(4) Ianniruberto, G.; Brasiello, A.; Marrucci, G. Friction coefficient does not stay constant in nonlinear viscoelasticity. *7th Annual European Rheology Conference*; University Federico: Suzdal, Russia, 2011; Vol. *61*.

(5) Ianniruberto, G.; Brasiello, A.; Marrucci, G. Simulations of fast shear flows of PS oligomers confirm monomeric friction reduction in fast elongational flows of monodisperse PS melts as indicated by rheooptical data. *Macromolecules* **2012**, *45* (19), 8058−8066.

(6) Yaoita, T.; Isaki, T.; Masubuchi, Y.; Watanabe, H.; Ianniruberto, G.; Marrucci, G. Primitive chain network simulation of elongational flows of entangled linear chains: Stretch/Orientation-induced reduction of monomeric friction. *Macromolecules* **2012**, *45* (6), 2773−2782.

(7) Luap, C.; Müller, C.; Schweizer, T.; Venerus, D. C. Simultaneous stress and birefringence measurements during uniaxial elongation of polystyrene melts with narrow molecular weight distribution. *Rheol. Acta* **2005**, *45* (1), 83−91.

(8) Marrucci, G.; Ianniruberto, G. Interchain pressure effect in extensional flows of entangled polymer melts. *Macromolecules* **2004**, *37* (10), 3934−3942.

(9) Wagner, M. H.; Narimissa, E. A new perspective on monomeric friction reduction in fast elongational flows of polystyrene melts and solutions. *J. Rheol.* **2021**, *65* (6), 1413−1421.

(10) Wagner, M. H.; Narimissa, E.; Masubuchi, Y. Elongational viscosity of poly(propylene carbonate) melts: tube-based modelling and primitive chain network simulations. *Rheol. Acta* **2023**, *62* (1), 1−14.

(11) Yang, L.; Uneyama, T.; Masubuchi, Y.; Doi, Y. Nonlinear shear and elongational rheology of poly(propylene carbonate). *Nihon Reoroji Gakkaishi* **2022**, *50* (1), 127−135.

(12) Matsumiya, Y.; Sato, T.; Chen, Q.; Watanabe, H. Rheo-dielectric behavior of unentangled poly (butylene oxide) under steady shear: Preliminary evaluation of non-equilibrium parameters at the onset of nonlinearity. *Nihon Reoroji Gakkaishi* **2022**, *50* (5), 371−385.

(13) Matsumiya, Y.; Sato, T.; Chen, Q.; Watanabe, H. Rouse Analysis of nonlinear rheology of unentangled polymer melts under fast shear: Viscoelastic response to superposed oscillatory strain. *Macromolecules* **2023**, *56* (8), 2930−2938.

(14) Jiang, N. Potential universal extensional rheology in concentrated polymeric liquids. *Macromolecules* **2024**, *57* (11), 5520−5532.

(15) André, A.; Shahid, T.; Oosterlinck, F.; Clasen, C.; Van Ruymbeke, E. Investigating the transition between polymer melts and solutions in nonlinear elongational flow. *Macromolecules* **2021**, *54* (6), 2797−2810.

(16) Morelly, S. L.; Palmese, L.; Watanabe, H.; Alvarez, N. J. Effect of finite extensibility on nonlinear extensional rheology of polymer melts. *Macromolecules* **2019**, *52* (3), 915−922.

(17) Matsumiya, Y.; Watanabe, Y.; Masubuchi, Y.; Huang, Q.; Hassager, O. Nonlinear elongational rheology of unentangled polystyrene and poly(p-tert-butylstyrene) melts. *Macromolecules* **2018**, *51* (23), 9710−9729.

(18) Costanzo, S.; Huang, Q.; Ianniruberto, G.; Marrucci, G.; Hassager, O.; Vlassopoulos, D. Shear and extensional rheology of polystyrene melts and solutions with the same number of entanglements. *Macromolecules* **2016**, *49* (10), 3925−3935.

(19) Huang, Q.; Agostini, S.; Hengeller, L.; Shivokhin, M.; Alvarez, N. J.; Hutchings, L. R.; Hassager, O. Dynamics of star polymers in fast extensional flow and stress relaxation. *Macromolecules* **2016**, *49* (17), 6694−6699.

(20) Huang, Q.; Alvarez, N. J.; Matsumiya, Y.; Rasmussen, H. K.; Watanabe, H.; Hassager, O. Extensional rheology of entangled polystyrene solutions suggests importance of nematic interactions. *ACS Macro Lett.* **2013**, *2* (8), 741−744.

(21) Huang, Q.; Mednova, O.; Rasmussen, H. K.; Alvarez, N. J.; Skov, A. L.; Almdal, K.; Hassager, O. Concentrated polymer solutions are different from melts: Role of entanglement molecular weight. *Macromolecules* **2013**, *46* (12), 5026−5035.

(22) Nielsen, J. K.; Rasmussen, H. K.; Hassager, O.; McKinley, G. H. Elongational viscosity of monodisperse and bidisperse polystyrene melts. *J. Rheol.* **2006**, *50* (4), 453−476.

(23) Nielsen, J. K.; Rasmussen, H. K.; Denberg, M.; Almdal, K.; Hassager, O. Nonlinear branch-point dynamics of multiarm polystyrene. *Macromolecules* **2006**, *39* (25), 8844−8853.

(24) Bach, A.; Almdal, K.; Rasmussen, H. K.; Hassager, O. Elongational viscosity of narrow molar mass distribution polystyrene. *Macromolecules* **2003**, *36* (14), 5174−5179.

(25) Bhattacharjee, P.; Oberhauser, J.; McKinley, G. H.; Leal, L.; Sridhar, T. Extensional rheometry of entangled solutions. *Macromolecules* **2002**, *35* (27), 10131−10148.

(26) Wagner, M. H.; Narimissa, E.; Huang, Q. Scaling relations for brittle fracture of entangled polystyrene melts and solutions in elongational flow. *J. Rheol.* **2021**, *65* (3), 311−324.

(27) Sridhar, T.; Acharya, M.; Nguyen, D. A.; Bhattacharjee, P. K. On the extensional rheology of polymer melts and concentrated solutions. *Macromolecules* **2014**, *47* (1), 379−386.

(28) Yang, L.; Uneyama, T.; Masubuchi, Y.; Doi, Y. Linear rheological properties of poly(propylene carbonate) with different molecular weights. *Nihon Reoroji Gakkaishi* **2021**, *49* (4), 267−274.
(29) Wu, S.; Yang, H.; Chen, Q. Nonlinear extensional rheology of poly(n-alkyl methacrylate) melts with a fixed number of Kuhn segments and entanglements per chain. *ACS Macro Lett.* **2022**, *11* (4), 484−490.
(30) Masubuchi, Y.; Yang, L.; Uneyama, T.; Doi, Y. Analysis of elongational viscosity of entangled poly(propylene carbonate) melts by primitive chain network simulations. *Polymers* **2022**, *14* (4), 741.
(31) Zhong, Y.; Liu, S.; Luo, L.; Huang, Q. Influence of chemical side groups containing aromatic rings: Flow-induced friction enhancement or reduction. *Macromolecules* **2024**, *57* (10), 4833−4841.
(32) Lopez-Barron, C. R.; Zhou, H. Extensional strain hardening induced by π-π interactions in Barely entangled polymer chains: The curious case of poly(4-vinylbiphenyl). *Phys. Rev. Lett.* **2017**, *119* (24), 247801.
(33) Lopez-Barron, C. R.; Burghardt, W. R.; Kweon, M. S. Local and global stretching of polymer chains during startup of extensional flow. *ACS Macro Lett.* **2020**, *9* (1), 26−31.
(34) López-Barrón, C. R.; Shivokhin, M. E. Extensional strain hardening in highly entangled molecular bottlebrushes. *Phys. Rev. Lett.* **2019**, *122* (3), 037801.
(35) López-Barrón, C. R.; Shivokhin, M. E.; Hagadorn, J. R. Extensional rheology of highly-entangled α-olefin molecular bottlebrushes. *J. Rheol.* **2019**, *63* (6), 917−926.
(36) Wagner, M. H.; Hirschberg, V. Rheology of poly(α-olefin) bottlebrushes: Effect of self-dilution by alkane side chains. *Macromolecules* **2024**, *57* (5), 2110−2118.
(37) Rasmussen, H. K.; Wingstrand, S. L.; Hassager, O. On the universality in the extensional rheology of monodisperse polymer melts and oligomer dilutions thereof. *Rheol. Acta* **2019**, *58* (6−7), 333−340.
(38) Zatloukal, M.; Drabek, J. Reduction of monomeric friction coefficient for linear isotactic polypropylene melts in very fast uniaxial extensional flow. *Phys. Fluids* **2021**, *33* (5), 051703.
(39) Münstedt, H. Various features of melt strain hardening of polymeric materials in uniaxial extension and their relation to molecular structure: review of experimental results and their interpretation. *Rheol. Acta* **2023**, *62* (7−8), 333−363.
(40) Tan, D. H.; Zhou, C.; Ellison, C. J.; Kumar, S.; Macosko, C. W.; Bates, F. S. Meltblown fibers: Influence of viscosity and elasticity on diameter distribution. *J. Non-Newtonian Fluid Mech.* **2010**, *165* (15−16), 892−900.
(41) Ellison, C. J.; Phatak, A.; Giles, D. W.; Macosko, C. W.; Bates, F. S. Melt blown nanofibers: fiber diameter distributions and onset of fiber breakup. *Polymer* **2007**, *48* (11), 3306−3316.
(42) Drabek, J.; Zatloukal, M. Meltblown technology for production of polymeric microfibers/nanofibers: A review. *Phys. Fluids* **2019**, *31* (9), 091301.
(43) Colby, R. H.; Fetters, L. J.; Grassley, W. W. Melt viscosity-molecular weight relationship for linear polymers. *Macromolecules* **1987**, *20* (9), 2226−2237.
(44) Colby, R. H.; Fetters, L. J.; Funk, W. G.; Grassley, W. W. Effects of concentration and thermodynamic interaction on the viscoelastic properties of polymer solutions. *Macromolecules* **1991**, *24* (13), 3873−3882.
(45) Chen, F.; Peng, D.; Ogata, Y.; Tanaka, K.; Yang, Z.; Fujii, Y.; Yamada, N. L.; Lam, C. H.; Tsui, O. K. C. Confinement effect on the effective viscosity of plasticized polymer films. *Macromolecules* **2015**, *48* (20), 7719−7726.
(46) Drabek, J.; Zatloukal, M.; Martyn, M. Effect of molecular weight on secondary Newtonian plateau at high shear rates for linear isotactic melt blown polypropylenes. *J. Non-Newtonian Fluid Mech.* **2018**, *251*, 107−118.
(47) Drabek, J.; Zatloukal, M.; Martyn, M. Effect of molecular weight, branching and temperature on dynamics of polypropylene melts at very high shear rates. *Polymer* **2018**, *144*, 179−183.
(48) Osaki, K.; Nishizawa, K.; Kurata, M. Material time constant characterizing the nonlinear viscoelasticity of entangled polymeric systems. *Macromolecules* **1982**, *15* (4), 1068−1071.
(49) Dealy, J. M.; Read, D. J.; Larson, R. G. *Structure and Rheology of Molten Polymers: From Structure to Flow Behavior and Back Again*; 2nd ed.; Hanser; Munich, 2018.
(50) Doi, M.; Edwards, S. F. *The Theory of Polymer Dynamics*; Oxford Science Publications Oxford: Clarendon Press, 1986.
(51) Watanabe, H. Viscoelasticity and dynamics of entangled polymers. *Prog. Polym. Sci.* **1999**, *24* (9), 1253−1403.
(52) Fetters, L. J.; Lohse, D. J.; Colby, R. *Chain Dimensions and Entanglement Spacings in Physical Properties of Polymers Handbook*, 2nd ed., Springer: New York, 2007; pp 447−454.
(53) Gibson, A. G. Die entry flow of reinforced polymers. *Composites* **1989**, *20* (1), 57−64.
(54) Zatloukal, M.; Vlcek, J.; Tzoganakis, C.; Saha, P. Improvement in techniques for the determination of extensional rheological data from entrance flows: Computational and experimental analysis. *J. Non-Newtonian Fluid Mech.* **2002**, *107* (1−3), 13−37.
(55) Zatloukal, M.; Musil, J. Analysis of entrance pressure drop techniques for extensional viscosity determination. *Polym. Test.* **2009**, *28* (8), 843−853.
(56) Drabek, J.; Zatloukal, M. Influence of long chain branching on fiber diameter distribution for polypropylene nonwovens produced by melt blown process. *J. Rheol.* **2019**, *63* (4), 519−532.
(57) Drabek, J.; Zatloukal, M. Influence of molecular weight, temperature, and extensional rheology on melt blowing process stability for linear isotactic polypropylene. *Phys. Fluids* **2020**, *32* (8), 083110.
(58) Kelly, A. L.; Gough, A. T.; Whiteside, B. R.; Coates, P. D. High shear strain rate rheometry of polymer melts. *J. Appl. Polym. Sci.* **2009**, *114* (2), 864−873.
(59) McKinley, G. H.; Raiford, W. P.; Brown, R. A.; Armstrong, R. C. Nonlinear dynamics of viscoelastic flow in axisymmetric abrupt contractions. *J. Fluid Mech.* **1991**, *223*, 411−456.
(60) Padmanabhan, M.; Macosko, C. W.; Padmanabhan, M. Extensional viscosity from entrance pressure drop measurements. *Rheol. Acta* **1997**, *36* (2), 144−151.
(61) Auhl, D.; Stadler, F. J.; Münstedt, H. Rheological properties of electron beam-irradiated polypropylenes with different molar masses. *Rheol. Acta* **2012**, *51* (11−12), 979−989.
(62) Auhl, D.; Stadler, F. J.; Münstedt, H. Comparison of molecular structure and rheological properties of electron-beam- and gamma-irradiated polypropylene. *Macromolecules* **2012**, *45* (4), 2057−2065.
(63) Auhl, D. Molekulare struktur und rheologische eigenschaften stranhlenmodifizierter polypropylene. Ph.D, Dissertation, Der Technischen Fakultät der Universität Erlangen-Nürnberg, Erlangen, Germany, 2006. https://open.fau.de/server/api/core/bitstreams/1a63d236-e72b-447c-bef2-d5c65f2a4e38/content.
(64) Münstedt, H.; Auhl, D. Rheological measuring techniques and their relevance for the molecular characterization of polymers. *J. Fluid Mech.* **2005**, *128* (1), 62−69.
(65) Doolittle, A. K. Studies in newtonian flow. II. the dependence of the viscosity of liquids on free-space. *J. Appl. Phys.* **1951**, *22* (12), 1471−1475.
(66) Doolittle, A. K.; Doolittle, D. B. Studies in Newtonian Flow. V. Further verification of the free-space viscosity equation. *J. Appl. Phys.* **1957**, *28* (8), 901−905.
(67) Ferry, J. D. *Viscoelastic Properties of Polymers*, 3rd ed.; John Wiley; New York, 1980.
(68) Cohen, M. H.; Turnbull, D. Molecular transport in liquids and glasses. *J. Chem. Phys.* **1959**, *31* (5), 1164−1169.
(69) Turnbull, D.; Cohen, M. H. Free-volume model of the amorphous phase: Glass transition. *J. Chem. Phys.* **1961**, *34* (1), 120−125.
(70) Williams, M. L.; Landel, R. F.; Ferry, J. D. The temperature dependence of relaxation mechanisms in amorphous polymers and other glass-forming liquids. *J. Am. Chem. Soc.* **1955**, *77* (14), 3701−3707.
(71) Ngai, K. L.; Plazek, D. J. Temperature dependences of the viscoelastic response of polymer systems. In *Physical Properties of*

https://doi.org/10.1021/acs.macromol.5c00660
Macromolecules 2025, 58, 6041−6051

Polymers Handbook; Mark, J. E., Ed.; Springer: New York, 2007; pp 455−478.
(72) Utracki, L. A.; Sedlacek, T. Free volume dependence of polymer viscosity. *Rheol. Acta* **2007**, *46* (4), 479−494.
(73) Schmidt, K. A. G.; Pagnutti, D.; Curran, M. D.; Singh, A.; Trusler, J. P. M.; Maitland, G. C.; McBride-Wright, M. New experimental data and reference models for the viscosity and density of squalane. *J. Chem. Eng. Data* **2015**, *60* (1), 137−150.
(74) Park, G. W.; Ianniruberto, G. Flow-induced nematic interaction and friction reduction successfully describe PS melt and solution data in extension startup and relaxation. *Macromolecules* **2017**, *50* (12), 4787−4796.

https://doi.org/10.1021/acs.macromol.5c00660
Macromolecules 2025, 58, 6041−6051